



Tool vibration, surface roughness, cutting power, and productivity assessment using RSM and GRA approach during machining of Inconel 718 with PVD-coated carbide tool

Ilyas Kouahla¹ · Mohamed Athmane Yaltese¹ · Salim Belhadi¹ · Khaoula Safi¹ · Mourad Nouioua^{1,2}

Received: 24 April 2022 / Accepted: 16 August 2022 / Published online: 27 August 2022
© The Author(s), under exclusive licence to Springer-Verlag London Ltd., part of Springer Nature 2022

Abstract

Nickel-based alloys such as (Inconel 718) are widely used in the fields of space technology, rocket engines, nuclear reactors, petrochemicals, submarines, power plants, and others. Due to its high mechanical properties, low thermal conductivity, and other characteristics, it is classified as a difficult material to machine. The main objective of this work is to model the tool vibration (V_{mg}), surface roughness (Ra), cutting force (F_z), power consumption (P_c), and material removal rate (MRR) as a function of different cutting conditions such as cutting speed (V_c), feed rate (f), depth of cut (ap), and tool nose radius (r). Machining tests were performed by dry turning of Inconel 718 with a PVD-coated metal carbide tool, following a Taguchi L_{27} (3^4) design of experiment. The response surface methodology (RSM) and the analysis of variance (ANOVA) were used to develop prediction models. The desirability function (DF) and the gray relational analysis (GRA) method were used and compared to determine the optimal cutting conditions, in order to minimize the outputs (V_{mg} , Ra , F_z , and P_c), and maximize the (MRR), according to two study cases encountered in industry.

Keywords Turning · Inconel 718 · Vibration · Surface roughness · Cutting power · Productivity · Modeling · Optimization

Abbreviations

PVD	Physical vapor deposition
TiAlN	Titanium nitride and aluminum coating
ANOVA	Analysis of variance
RSM	Response surface methodology
R^2	Coefficient of determination
V_{mg}	Tangential vibration (m/s^2)
Ra	Surface roughness (μm)
F_z	Tangential cutting force (N)
P_c	Power consumption (W)
MRR	Material removal rate (cm^3/min)
r	Tool nose radius (mm)
r	Tool nose radius (mm)
f	Feed rate (mm/rev)
ap	Depth of cut (mm)

df	Degrees of freedom
Séq SS	Sequential sums of squares
Cont%	Contribution percentage
TOPSIS	Technique for Order Preference by Similarity to Ideal Solution
Adj SS	Adjusted sums of squares
Adj MS	Adjusted mean squares
F value	Fisher's coefficient
P value	Probability value
DF	Desirability function
GRA	Grey relational analysis
ANN	Artificial neural network
MCDM	Multiple criteria decision making
ARAS	Additive ratio assessment system
CODAS	Combinative distance-based assessment
PSO	Particle swarm optimization
GA	Genetic algorithm
EDM	Electrical discharge machining
ASCF	Atomized spray cutting fluid
SVM	Support vector machine
FL	Fuzzy logic
PCA	Principal component analysis

✉ Ilyas Kouahla
ilyaskouahla@gmail.com

¹ Department of Mechanical Engineering, Mechanics and Structure Laboratory (LMS), Université 8 Mai 1945, BP 401, 24000 Guelma, Algeria

² Mechanics Research Center, Po. Box 73B, 25021 Constantine, Algeria

1 Introduction

Inconel is a refractory superalloy that contains a large amount of nickel and chromium. It is used in many technological applications because of its mechanical performance at relatively high temperatures up to 650 °C. Because of the low thermal conductivity, machining of this material is characterized by rapid wear of the cutting tools, poor surface quality, high cutting forces, and high vibrations [1]. For these reasons, Inconel is classified as a difficult material to machine. This is why this refractory alloy has aroused a great deal of interest in the scientific community and particularly in the field of machining [2]. A lot of research has been done on the machining of this material in order to find the optimal conditions that guarantee easy machining, high surface quality, minimum energy consumption, and maximum productivity at low cost [3, 4]. Devillez et al. [5] performed surface integrity tests when machining Inconel 718 with and without lubrication using a carbide metal tool. The results found show that dry machining with a coated carbide tool leads to potentially acceptable surface quality with residual stresses and microhardness values of the same order as those obtained under wet conditions using the optimized (V_c) value. Cantero et al. [6] analyzed the mechanisms of tool wear (cemented carbide, ceramic, and CBN) when turning Inconel 718. Park et al. [7] evaluated cutting tool wear in different lubrication environments when machining Inconel 718. Rahman et al. [8] examined the effect of cutting conditions on the machinability of Inconel 718. Wear (V_b), workpiece roughness (R_a), and cutting force (F_z) were used as performance indicators for tool life. Mahesh et al. [9] presented a detailed literature review of heat generation during machining of Inconel 718 and its influence on various output machining parameters. The study was interested in the multiple possibilities to reduce the cutting temperature. Behera et al. [10] investigated the dry machining performance of Inconel 825 (difficult to cut) using uncoated carbide and MT-CVD TiCN- Al_2O_3 -coated carbide inserts. The results reveal that the coated tool results in a 39.79% reduction in tangential cutting force at ($V_c = 121$ m/min). Deshpande et al. [11] developed surface roughness prediction models considering cutting parameters, cutting force, sound, and vibration during turning of Inconel 718 with cryogenic and non-treated. Tebassi et al. [12] performed a modeling study of (R_a) and (MRR) when turning Inconel 718 (35 HRC) with the ceramic tool ($Al_2O_3 + SiC$ Whisker). Thirumalai et al. [13] applied the method (TOPSIS) to optimize the cutting parameters during turning of Inconel 718. Deshpande et al. [14] used the (ANN) method to predict roughness (R_a) using cutting parameters, cutting force, sound, and vibration when turning Inconel 718. The authors confirm that the developed (ANN) models predict (R_a) with more than 98% precision.

Recently, in (2022), several other researches have been performed on Inconel machining, among them are the following: (1) Tan et al. [15] performed a turning study on the surface integrity of Inconel 718 machined by two carbide and ceramic inserts. The effects of cutting parameters on surface roughness, residual stresses, and micro-hardness were considered. (2) Alsuruji et al. [16] proposed the Taguchi analysis coupled with the (GRA) method for obtaining an optimal cutting regime that satisfies high (MRR), lower taper angle, and minimum roughness, in laser beam drilling of Inconel 718. (3) Xu et al. [17] presented an experimental and numerical investigation during the machining of Inconel 718 with worn tools. Chip formation, cutting force variation, tool wear and thermal distribution, and microstructure were examined. (4) Sivalingam et al. [18] exploited two methods (MCDM), namely (ARAS) and (CODAS) in order to optimize the operating parameters when turning Inconel 718 alloy in dry cutting environments and (ASCF). (5) Zahoor et al. [19] compared three optimization methods (PSO, GA, and DF) to minimize (R_a) when milling Inconel 718. The results found reveal that the optimization approach (PSO) is more efficient than the methods (GA and DF).

Optimization in the machining process is considered to be a very important operation that allows the proper choice of cutting conditions in order to improve productivity, ensure the quality of the final product, and reduce the manufacturing cost. The optimization methods applied in machining are numerous [20, 21] and their effectiveness varies from one method to another. The (DF) approach is a multi-objective optimization method, which has been widely used by many researchers in many fields, particularly in machining optimization [22]. Frifita et al. [23], Tebassi et al. [24], Parida and Maity [25], Kuppan et al. [26], Kar et al. [27], Manohar et al. [28], and Świercz et al. [29], have used it successfully in machining Inconel. On the other hand, the (GRA) method is among the most widely used optimization ones in several fields of science and particularly in the field of mechanical manufacturing. This method has proved its effectiveness in determining the optimal operating conditions in machining in order to overcome the problem of multi-response optimization [30]. Karsh and Singh [31] and Sanghvi et al. [32] applied the (GRA) method while machining 625 and 825 Inconel to solve the multi-objective optimization problems of cutting conditions in (EDM). Vikram et al. [33] evaluated the process parameters with (GRA) analysis when machining low machinability materials under dry and wet conditions. Sahu et al. [34] used the (GRA) method for process parameter optimization in electrostatic discharge machining of titanium alloy (Ti6Al4V) and 316L stainless steel. Kant and Dhama [35] performed a multi-response optimization of the parameters using the (GRA) method during abrasive waterjet machining of EN31 steel. Moharana and Patro [36] realized a multi-objective optimization of the machining

parameters of EN-8 carbon steel in (EDM) using the (GRA) method. Also, Pradhan [37] and Hanif et al. [38] applied the (RSM and GRA) methods during (EDM) machining of AISI D2 steel to optimize the operating factors. Also, Chaudhari et al. [39] exploited the two approaches (RSM and GRA) coupled with the (PCA) method to find the optimal parameters during (EDM) machining of pure titanium. In order to find the optimal parameters when milling a glass fiber-reinforced polymer, Yaser and Shunmugesh [40] successfully employed the approaches (GRA and DF).

A literature review shows that very few studies have been conducted on the machining of Inconel 718 by a PVD-coated carbide insert, taking into account the tool vibration parameter. Also, the analysis of the literature shows that very little research has been carried out on the machining of Inconel 718 by introducing four input factors and five output technological parameters simultaneously, which constitutes the originality of this work. Moreover, in this machining context, almost no study has considered a comparison between two optimization methods, namely the desirability function (DF) based on regression models and the method (GRA) derived from methods multiple criteria decision (MCDM) according to several desired cases.

The main objective of this article is to develop mathematical prediction models for the output parameters (V_{tng} , Ra , F_z , P_c , and MRR) using the approach (RSM) and analysis (ANOVA) in order to quantify the influence of the input factors (V_c , f , ap , and r) on the outputs when turning Inconel 718 according to a Taguchi orthogonal array L_{27} (3^4). Moreover, the (DF) and (GRA) approaches were used and compared in order to perform a multi-objective optimization according to two case studies that can be encountered in the industry. The proposed work concerns all mechanical manufacturing companies, as it provides the information necessary for the analysis of product quality.

2 Experimental procedure

2.1 Couple tool/material to be machined

The material used in this study is the refractory alloy (Inconel 718). It is widely used in the marine, nuclear, space technology, rocket engine, nuclear reactors, petrochemical, submarine, and power plant sectors. The specimen used is a cylindrical bar with a diameter of 70 mm and a length of 350 mm. The chemical composition of Inconel 718 is given in Table 1. The turning tests were performed on a conventional lathe (TOS TRENCIN) model SN40C ($P_m = 6.6$ kW) following the standard (ISO 3685). The lathe is equipped with a variable speed drive, model ABB series ACS355, with a speed sensor allowing the control of the speed of rotation of the spindle. The cutting inserts

Table 1 Chemical composition of Inconel 718 (%)

Element	Quantity %	Element	Quantity %	Element	Quantity %
C	0.08	Mo	3.3	Ni + Co	55
Co	1	P	0.015	Al	0.8
Mn	0.35	Ti	1.15	Cr	21
Fe	12.29	S	0.015	Cb + Ta	5.5
Sn	0.35	Cu	0.15		

used are metal carbide with a (PVD) coating of grade (GC1105) from the firm SANDVIK. The (PVD) coating consists of a thin layer of TiAlN offering high tenacity, excellent adhesion, and even draft wear [41]. The inserts are mounted on a SANDVIK tool holder with the ISO designation PSBNR2525K12 (Fig. 1).

2.2 Measuring equipment

Figure 2 exposes the equipment used for the measurement of the different output parameters. The measurement of roughness (Ra) was performed by a roughness meter (2D) of the MITUTOYO model SJ-210. It consists of a 5- μ m diamond tip (feeler) that moves axially over a distance of 4 mm on the machined surface. Measurements were repeated three times by flipping the workpiece through a 120° angle and the average of the measurements was taken. The acquisition of the roughness profiles was performed with a roughness meter software (SJ- Communication-Tool) (Fig. 2a). In order to measure the vibrations of the tool in the tangential direction (V_{tng}), a vibrometer type VM-6360 accompanied by an accelerometer was used. The acquisition of the measurements was performed using the program (data collection system) (Fig. 2b). To measure the tangential cutting force (F_z) generated during machining, a dynamometer (KISTLER 9257 B) was used (Fig. 2c). The power consumed during machining (P_c) was calculated based on the tangential force (F_z) measured according to Eq. (1). The material removal rate (MRR) was chosen as an index of productivity; it was calculated according to Eq. (2).

$$P_c = \frac{F_z \cdot V_c}{60}, [W] \quad (1)$$

$$MRR = V_c \cdot f \cdot ap [cm^3/min] \quad (2)$$

2.3 Experimental design

The standard Taguchi L_{27} (3^4) orthogonal table was adopted as the experimental design. Four input factors were chosen: the first one was assigned to the tool nose radius (r), the second to the cutting speed (V_c), the third to the feed

Fig. 1 Machine, tool, and material used



rate per revolution (f), and the last to the depth of cut (ap). Each factor varied in three levels, and the range of variation is shown in Table 2. The choice of cutting conditions is made according to the recommendations of the cutting tool manufacturer (SANDVIK). The design of the experiment's matrix, adopted according to Taguchi L27 design, gives the different combinations of input factors as it is shown in Table 3.

3 Results and discussion

Table 3 presents the experimental values of the output parameters as a function of the four main cutting factors (r , V_c , f , and ap). These values were obtained as a result of the different combinations of the elements of the cutting regime according to Taguchi orthogonal array L₂₇ during turnings of Inconel 718. After the analysis of the obtained values, it can be seen that the roughness (Ra) varies from (0.296 to 0.929 μm), the tool vibration (V_{mg}) varies from (1.334 to 3.728 m/s^2), the tangential force (F_z) varies from (49.640 to 217.050 N), while the power consumption (P_c) varies from

(27.900 to 181.755 W), and for the material removal rate (MRR), it varies from (0.240 to 2.240 cm^3/min).

3.1 Analysis of variance (ANOVA)

In order to make the statistical study and determine the contribution of the main factors and the interactions, ANOVA was exploited. The results from the ANOVA for the four output parameters (Ra , V_{mg} , F_z , and P_c) were obtained for a significance level ($\alpha = 0.05$), which means a confidence level of 95%. In the ANOVA tables, the values of the degrees of freedom (df) are reported; the sequential sum of squares (SS_{Seq}) was used to quantify the variation in response data explained by each term. Column 3 shows the values of the contributions of the input factors on the output parameters (cont%), followed by the sum of adjusted squares ($Adj SS$), and then the mean squares ($Adj MS$). Fisher's coefficient (F value) and probability value (P value) indicate the level of significance of the factors for each of the output parameters. If $P > 0.05$, the factor is statistically insignificant on the measured response. On the other hand, if $P < 0.05$, the factor is statistically significant.

Fig. 2 Equipment used for experimental measurements



a). *Mitutoyo SurfTest SJ-210 2D roughness tester with runtime software.*



b). *Vibrometer, VM 6360 Digital Vibration Tester + Accelerator with running software.*



c). *Dynamometer (KISTLER 9257 B) with kistler signal amplifiers, acquisition board and dynoware measurement program.*

3.1.1 ANOVA for (Ra) and (Vtng)

The results of the ANOVA of (Ra) are indicated in Table 4. The main factors are significant because $P < 0.05$. The

Table 2 Levels of entry factors

Entry factors		Level 1	Level 2	Level 3
Tool nose radius	r (mm)	0.8	1.2	1.6
Cutting speed	V_c (m/min)	30	50	70
Feed rate	f (mm/rev)	0.08	0.12	0.16
Depth of cut	a_p (mm)	0.1	0.2	0.3

feed rate (f) has a great influence on the criterion (Ra) with (23.39%) of cont%, followed by (V_c) with (16.09%) of cont%, then comes the factors (r and a_p) with (3.7% and 0.02%) of cont% respectively. The square term ($V_c \times V_c$) is significant with (3.61%) of cont%. The interactions ($r \times V_c$), ($r \times f$), ($V_c \times f$), and ($V_c \times a_p$) are also significant with (3.81%, 19.42%, 4.13%, and 4.97%) of cont% respectively. These results are in perfect agreement with those [24, 42–44]. Table 5 shows the ANOVA of the tangential vibration (Vtng). It can be seen that all three factors (r , V_c , and a_p) are significant ($P < 0.05$). Radius (r) and speed (V_c) have the greatest influence with (32.41%) and (31.36%)

Table 3 Experimental results of performance parameters

No. of test	Input parameters				Output parameters				
	r (mm)	V_c (m/min)	f (mm/rev)	ap (mm)	R_a (μm)	V_{mg} (m/s^2)	F_z (N)	P_c (W)	MRR (cm^3/min)
1	0.8	30	0.08	0.1	0.401	2.077	55.800	27.900	0.240
2	0.8	30	0.12	0.2	0.571	2.247	118.450	59.225	0.720
3	0.8	30	0.16	0.3	0.672	2.691	190.540	95.270	1.440
4	0.8	50	0.08	0.2	0.328	1.334	76.870	64.058	0.800
5	0.8	50	0.12	0.3	0.349	2.142	144.950	120.792	1.800
6	0.8	50	0.16	0.1	0.787	1.603	63.770	53.142	0.800
7	0.8	70	0.08	0.3	0.280	1.828	121.850	142.158	1.680
8	0.8	70	0.12	0.1	0.338	1.484	49.640	57.913	0.840
9	0.8	70	0.16	0.2	0.435	2.106	147.750	172.375	2.240
10	1.2	30	0.08	0.1	0.457	2.870	85.270	42.635	0.240
11	1.2	30	0.12	0.2	0.431	3.537	116.965	58.483	0.720
12	1.2	30	0.16	0.3	0.582	3.728	217.050	108.525	1.440
13	1.2	50	0.08	0.2	0.386	2.865	84.300	70.250	0.800
14	1.2	50	0.12	0.3	0.433	2.673	173.080	144.233	1.800
15	1.2	50	0.16	0.1	0.649	2.037	93.400	77.833	0.800
16	1.2	70	0.08	0.3	0.428	2.428	120.820	140.957	1.680
17	1.2	70	0.12	0.1	0.282	2.012	67.610	78.878	0.840
18	1.2	70	0.16	0.2	0.476	2.440	146.000	170.333	2.240
19	1.6	30	0.08	0.1	0.394	3.393	83.220	41.610	0.240
20	1.6	30	0.12	0.2	0.390	3.683	134.530	67.265	0.720
21	1.6	30	0.16	0.3	0.464	3.535	212.100	106.050	1.440
22	1.6	50	0.08	0.2	0.434	2.157	103.690	86.408	0.800
23	1.6	50	0.12	0.3	0.445	2.839	169.020	140.850	1.800
24	1.6	50	0.16	0.1	0.457	2.400	89.160	74.300	0.800
25	1.6	70	0.08	0.3	0.433	2.579	123.540	144.130	1.680
26	1.6	70	0.12	0.1	0.357	2.383	84.460	98.537	0.840
27	1.6	70	0.16	0.2	0.284	2.588	155.790	181.755	2.240

cont% respectively, then followed by (ap) with (8.77%) cont%. Concerning the square terms ($r \times r$) and ($V_c \times V_c$), they are also significant with (6.23% and 9.41%) of cont% respectively. The rest of the terms do not have a significant influence on (V_{mg}). Almost similar results were found by Meddour et al. [45], when following the vibration in turning by taking into consideration the cutting conditions and tool nose radius.

3.1.2 ANOVA for (F_z) and (P_c)

Table 6 presents the results of the ANOVA for effort (F_z). It can be seen that the main factors are significant, as ($P < 0.05$). The principal contribution (64.11%) is attributed to the factor (ap), it is followed by (f) with (21.18%) of cont%, then follows the factors (V_c and r) with (3.86% and 3.46%) of cont% respectively. The square terms ($V_c \times V_c$), ($f \times f$), and ($ap \times ap$) are significant (cont% < 1.85%). Many researchers claim that the chip cross section ($ap \times f$) is the main factor affecting the stress (F_z) [44, 46, 47]. The

interactions ($V_c \times f$) and ($V_c \times ap$) are also significant with cont% of (2.13% and 1.08%) respectively. Concerning the results of (P_c) (Table 7), it is clear that the factors (ap) and (V_c) have the greatest influence with (38.29%) and (36.99%) cont% respectively. These results are very logical, since Eq. (1) indicates that speed (V_c) and effort (F_z) are the main factors controlling (P_c) [48, 49]. The other main factors (f and r) are significant with (8.59% and 2.41%) of cont%. The square term ($V_c \times V_c$) and the interaction ($V_c \times f$) are also significant with cont% of (0.62% and 9.22%).

3.1.3 Main effects plot and contributions

Figure 3 shows the plot of the main effects of the input factors (r , V_c , f , and ap) on the parameters (R_a , V_{mg} , F_z , and P_c). It is clearly seen in Fig. 3a, that the factors (f , V_c , and r) strongly affect (R_a) respectively, as they have high slopes. In contrast, the factor (ap) does not have a significant effect on (R_a). These results confirm the ANOVA results in Table 4. Several researches confirm that (ap) has little influence

Table 4 ANOVA for (*Ra*)

<i>Source</i>	<i>df</i>	<i>Seq SS</i>	<i>Cont%</i>	<i>Adj SS</i>	<i>Adj MS</i>	<i>F value</i>	<i>P value</i>
<i>Model</i>	13	0.349701	92.02%	0.349701	0.026900	11.53	0.000
<i>Linear</i>	4	0.164163	43.20%	0.173202	0.043301	18.57	0.000
<i>r</i>	1	0.014056	3.70%	0.014056	0.014056	6.03	0.029
<i>Vc</i>	1	0.061133	16.09%	0.061133	0.061133	26.21	0.000
<i>f</i>	1	0.088901	23.39%	0.094864	0.094864	40.67	0.000
<i>ap</i>	1	0.000072	0.02%	0.017248	0.017248	7.40	0.018
<i>Square</i>	4	0.051927	13.66%	0.021784	0.005446	2.33	0.110
<i>r × r</i>	1	0.003408	0.90%	0.003408	0.003408	1.46	0.248
<i>Vc × Vc</i>	1	0.013728	3.61%	0.013728	0.013728	5.89	0.031
<i>f × f</i>	1	0.024704	6.50%	0.004544	0.004544	1.95	0.186
<i>ap × ap</i>	1	0.010086	2.65%	0.000003	0.000003	0.00	0.973
<i>2-factor interaction</i>	5	0.133612	35.16%	0.133612	0.026722	11.46	0.000
<i>r × Vc</i>	1	0.014491	3.81%	0.014491	0.014491	6.21	0.027
<i>r × f</i>	1	0.073790	19.42%	0.073790	0.073790	31.64	0.000
<i>r × ap</i>	1	0.010740	2.83%	0.010740	0.010740	4.60	0.051
<i>Vc × f</i>	1	0.015708	4.13%	0.031417	0.031417	13.47	0.003
<i>Vc × ap</i>	1	0.018883	4.97%	0.018883	0.018883	8.10	0.014
<i>Error</i>	13	0.030321	7.98%	0.030321	0.002332		
<i>Total</i>	26	0.380022	100.00%				

on (*Ra*) during machining [23, 50]. For vibration (*Vtng*), the plots in Fig. 3b show that the factors (*Vc* and *r*) have a significant effect on (*Vtng*) because they have high slopes. While (*ap*) comes third, while the feed rate (*f*) does not have a significant effect on (*Vtng*). The slope analysis of the main effects of (*Fz*) Fig. 3c, shows that (*ap*) strongly affects (*Fz*),

followed by the feed rate (*f*), as they have the largest slope. Regarding the parameter (*Pc*) shown in Fig. 3d, we notice that (*ap*, *Vc*, and *f*) respectively strongly affect (*Pc*), while (*r*) has a smaller effect on (*Pc*). Figure 4 summarizes the different contributions of the main factors on the output parameters.

Table 5 ANOVA for (*Vtng*)

<i>Source</i>	<i>df</i>	<i>Seq SS</i>	<i>Cont%</i>	<i>Adj SS</i>	<i>Adj MS</i>	<i>F value</i>	<i>P value</i>
<i>Model</i>	13	10.3120	92.96%	10.3120	0.79323	13.20	0.000
<i>Linear</i>	4	8.1885	73.82%	8.0258	2.00645	33.40	0.000
<i>r</i>	1	3.5957	32.41%	3.5957	3.59567	59.85	0.000
<i>Vc</i>	1	3.4786	31.36%	3.4786	3.47864	57.90	0.000
<i>f</i>	1	0.1417	1.28%	0.0851	0.08507	1.42	0.255
<i>ap</i>	1	0.9725	8.77%	0.6861	0.68614	11.42	0.005
<i>Square</i>	4	1.7962	16.19%	1.7675	0.44188	7.36	0.003
<i>r × r</i>	1	0.6916	6.23%	0.6916	0.69156	11.51	0.005
<i>Vc × Vc</i>	1	1.0442	9.41%	1.0442	1.04417	17.38	0.001
<i>f × f</i>	1	0.0333	0.30%	0.0310	0.03100	0.52	0.485
<i>ap × ap</i>	1	0.0272	0.25%	0.0025	0.00252	0.04	0.841
<i>2-factor interaction</i>	5	0.3272	2.95%	0.3272	0.06545	1.09	0.411
<i>r × Vc</i>	1	0.1786	1.61%	0.1786	0.17861	2.97	0.108
<i>r × f</i>	1	0.0490	0.44%	0.0490	0.04902	0.82	0.383
<i>r × ap</i>	1	0.0432	0.39%	0.0432	0.04320	0.72	0.412
<i>Vc × f</i>	1	0.0551	0.50%	0.0343	0.03432	0.57	0.463
<i>Vc × ap</i>	1	0.0013	0.01%	0.0013	0.00130	0.02	0.885
<i>Error</i>	13	0.7810	7.04%	0.7810	0.06008		
<i>Total</i>	26	11.0930	100.00%				

Table 6 ANOVA for (F_z)

Source	df	Seq SS	Cont%	Adj SS	Adj MS	F value	P value
Model	13	54,610.1	98.32%	54,610.1	4200.8	58.58	0.000
Linear	4	51,440.6	92.61%	41,396.9	10,349.2	144.31	0.000
<i>r</i>	1	1919.7	3.46%	1919.7	1919.7	26.77	0.000
<i>Vc</i>	1	2144.4	3.86%	2144.4	2144.4	29.90	0.000
<i>f</i>	1	11,765.8	21.18%	3528.9	3528.9	49.21	0.000
<i>ap</i>	1	35,610.7	64.11%	26,624.2	26,624.2	371.26	0.000
Square	4	1215.3	2.19%	1754.1	438.5	6.11	0.005
<i>r</i> × <i>r</i>	1	130.2	0.23%	130.2	130.2	1.82	0.201
<i>Vc</i> × <i>Vc</i>	1	1021.9	1.84%	1021.9	1021.9	14.25	0.002
<i>f</i> × <i>f</i>	1	53.0	0.10%	343.6	343.6	4.79	0.047
<i>ap</i> × <i>ap</i>	1	10.1	0.02%	333.6	333.6	4.65	0.050
2-factor interaction	5	1954.3	3.52%	1954.3	390.9	5.45	0.006
<i>r</i> × <i>Vc</i>	1	35.1	0.06%	35.1	35.1	0.49	0.497
<i>r</i> × <i>f</i>	1	0.1	0.00%	0.1	0.1	0.00	0.975
<i>r</i> × <i>ap</i>	1	135.4	0.24%	135.4	135.4	1.89	0.193
<i>Vc</i> × <i>f</i>	1	1185.5	2.13%	1768.0	1768.0	24.65	0.000
<i>Vc</i> × <i>ap</i>	1	598.3	1.08%	598.3	598.3	8.34	0.013
Error	13	932.3	1.68%	932.3	71.7		
Total	26	55,542.4	100.00%				

3.2 Modeling of technological performance parameters

The relationship between input factors (*r*, *Vc*, *f*, and *ap*) and output parameters (*Ra*, *Ving*, *Fz*, and *Pc*) was modeled by quadratic regression equations. Insignificant terms were not

excluded from the equations in order to keep the (R^2) high. The different mathematical models found and their (R^2) are given by Eqs. (3), (4), (5) and (6). These models will be used for the prediction of the output parameters, in the range of variation of the cutting conditions and also for the optimization studies.

Table 7 ANOVA for (P_c)

Source	df	Seq SS	Cont%	Adj SS	Adj MS	F value	P value
Model	13	49,860.5	98.65%	49,860.5	3835.4	73.17	0.000
Linear	4	43,604.1	86.27%	46,848.8	11,712.2	223.45	0.000
<i>r</i>	1	1218.1	2.41%	1218.1	1218.1	23.24	0.000
<i>Vc</i>	1	18,693.7	36.99%	18,693.7	18,693.7	356.65	0.000
<i>f</i>	1	4339.3	8.59%	3044.8	3044.8	58.09	0.000
<i>ap</i>	1	19,353.1	38.29%	18,460.1	18,460.1	352.19	0.000
Square	4	1265.2	2.50%	521.9	130.5	2.49	0.095
<i>r</i> × <i>r</i>	1	47.3	0.09%	47.3	47.3	0.90	0.360
<i>Vc</i> × <i>Vc</i>	1	314.2	0.62%	314.2	314.2	6.00	0.029
<i>f</i> × <i>f</i>	1	402.0	0.80%	127.3	127.3	2.43	0.143
<i>ap</i> × <i>ap</i>	1	501.7	0.99%	50.7	50.7	0.97	0.343
2-factor interaction	5	4991.2	9.88%	4991.2	998.2	19.04	0.000
<i>r</i> × <i>Vc</i>	1	31.5	0.06%	31.5	31.5	0.60	0.452
<i>r</i> × <i>f</i>	1	0.9	0.00%	0.9	0.9	0.02	0.898
<i>r</i> × <i>ap</i>	1	151.8	0.30%	151.8	151.8	2.90	0.113
<i>Vc</i> × <i>f</i>	1	4659.0	9.22%	2812.3	2812.3	53.65	0.000
<i>Vc</i> × <i>ap</i>	1	147.9	0.29%	147.9	147.9	2.82	0.117
Error	13	681.4	1.35%	681.4	52.4		
Total	26	50,541.9	100.00%				

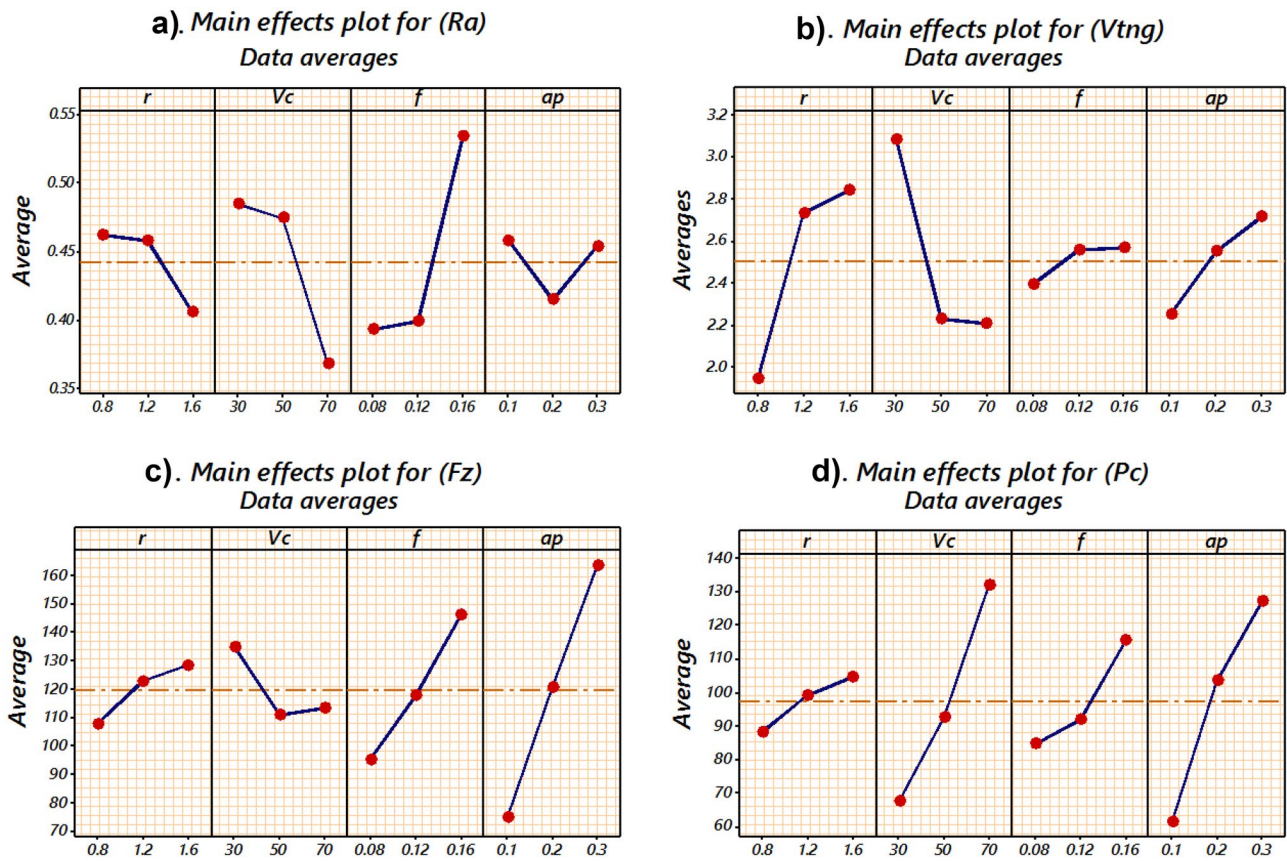


Fig. 3 Main effects plot for (Ra, Vtng, Fz, and Pc)

$$\begin{aligned}
 Ra[\mu\text{m}] = & -0.320 + 0.509r + 0.0099Vc + 8.90f - 2.92ap \\
 & - 0.149r^2 - 0.00012Vc^2 + 19.9f^2 - 0.08ap^2 \\
 & + 0.0043r \times Vc - 4.901r \times f + 0.748r \times ap \\
 & - 0.1044Vc \times f + 0.0324Vc \times ap
 \end{aligned} \tag{3}$$

$$R^2 = 92.02\%$$

$$\begin{aligned}
 Vtng[\text{m/s}^2] = & -0.96 + 7.75r - 0.1228Vc + 14.2f + 5.08ap \\
 & - 2.122r^2 + 0.001043Vc^2 - 51.9f^2 - 2.4ap^2 \\
 & - 0.01525r \times Vc - 3.99r \times f - 1.50r \times ap + 0.109Vc \\
 & \times f + 0.0085Vc \times ap
 \end{aligned} \tag{4}$$

$$R^2 = 92.96\%$$

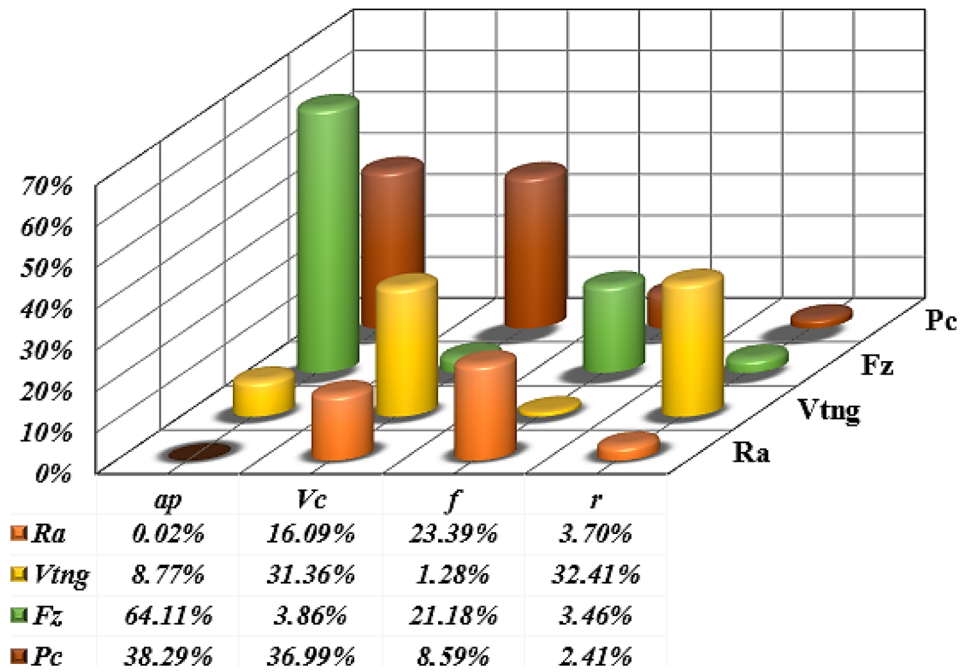
$$\begin{aligned}
 Fz[\text{N}] = & 140.6 + 123.8r - 5.37Vc - 2049f + 589ap - 29.1r^2 \\
 & + 0.03263Vc^2 + 5461f^2 + 861ap^2 - 0.214r \times Vc \\
 & - 5r \times f - 84.0r \times ap + 24.78Vc \times f - 5.77Vc \times ap
 \end{aligned} \tag{5}$$

$$R^2 = 98.32\%$$

$$\begin{aligned}
 Pc[\text{W}] = & 128.2 + 68.3r - 4.764Vc - 1921f + 282ap - 17.5r^2 \\
 & + 0.01809Vc^2 + 3324f^2 + 336ap^2 + 0.203r \times Vc \\
 & + 17r \times f - 88.9r \times ap + 31.25Vc \times f + 2.87Vc \times ap
 \end{aligned} \tag{6}$$

$$R^2 = 98.45\%$$

Fig. 4 Cont% of the main factors according to the output parameters



3.2.1 Experimental and predicted values and the probability diagram

Figure 5a–d compare the experimental and predicted values by the models found (Eqs. (3)–(6)). It can be seen, that the difference between the values is minimal and which implies a good correlation because all (R^2) varies between [92.02 and 98.45%]. Figure 6a–d present the normal probability plot for the parameters (*Ra*, *Vtng*, *Fz*, and *Pc*). We note that the regression model is statistically significant, as the majority of the residual values are almost aligned on a straight line, which led to the conclusion that the associated errors were normally distributed.

3.2.2 3D response surface

(a) 3D response surface for (*Ra*) and (*Vtng*)

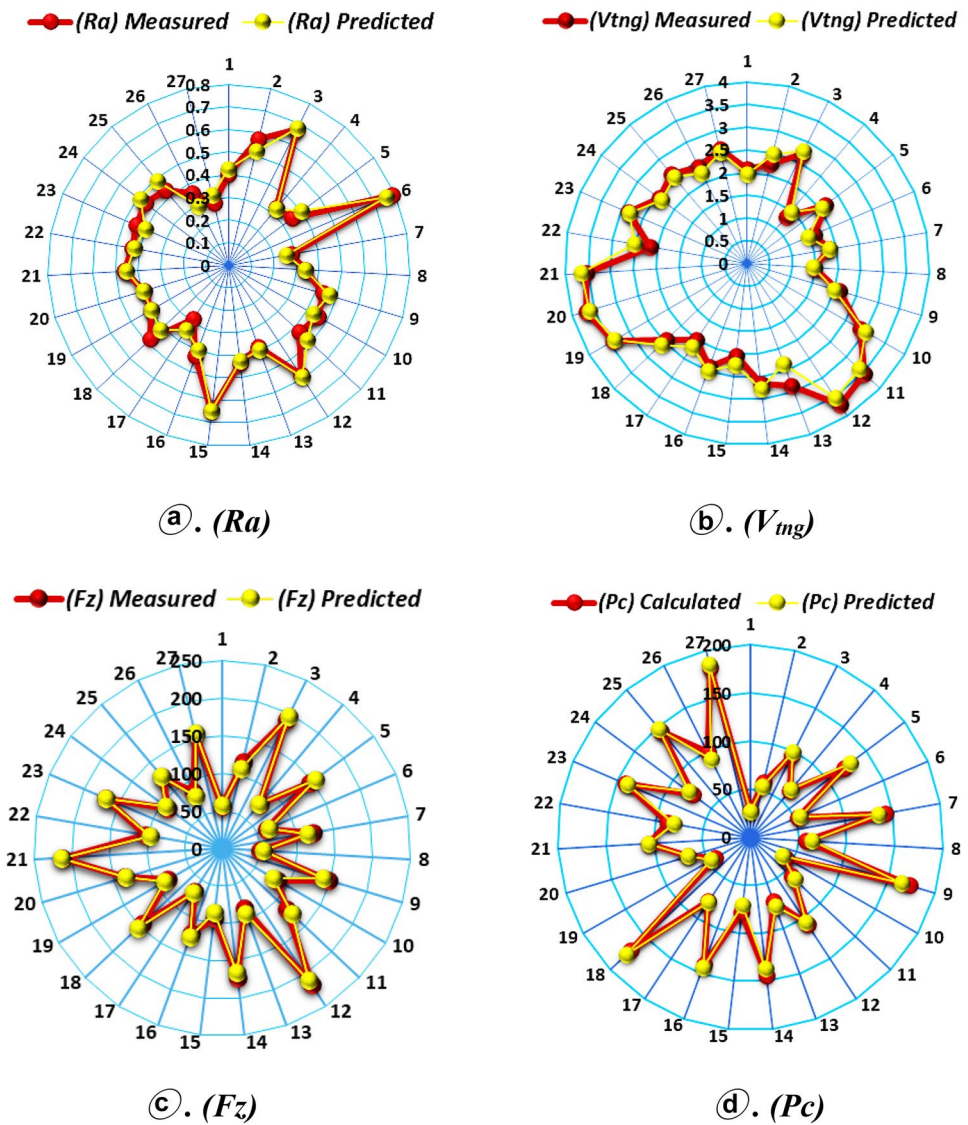
The 3D graphs of Fig. 7a–c allow to evaluate the simultaneous influence of ($f \times r$) ($f \times Vc$), and ($f \times ap$) on (*Ra*). We notice on Fig. 7a, that for a minimal value of (*f*), the radius (*r*) has almost no effect on (*Ra*). An increase in (*f*) leads to an increase in (*Ra*). But it should be noted that for a large feed, the increase in (*r*) allows a clear improvement in (*Ra*). It can be seen from Fig. 7b that for a minimum value of (*f*), the factor (*Vc*) has a very slight effect on the evolution of (*Ra*). On the other hand, for a maximum value of (*f*), an increase of (*Vc*) leads to a reduction of the criterion (*Ra*). Figure 6c shows that the minimum value of (*Ra*) is obtained with

minimum (*f*) and maximum (*ap*). The 3D plots in Fig. 8a–c permit to evaluate the simultaneous influence of ($Vc \times r$), ($Vc \times f$) and ($Vc \times ap$) on the vibration (*Vtng*). Figure 8a indicates that the factor (*Vc*) and (*r*) possess almost the same effect on (*Vtng*). It can be observed from Fig. 8(b) that (*Vc*) has a more pronounced influence on (*Vtng*) compared to that of (*f*); minimum values of the parameter (*Vtng*) are achieved for high values of (*Vc*). This is probably due to the reduction of the force (*Fz*). The minimum value of (*Vtng*) is obtained with (*Vc*) maximum and (*ap*) minimum Fig. 8c. These different 3D curves, prove the inexistence of interaction effect between the different input parameters considered on the variation of (*Vtng*). This was already found by the ANOVA analysis.

(b) 3D response surface for (*Fz*) and (*Pc*)

The 3D plots in Fig. 9a–c permit to evaluate the simultaneous influence of ($ap \times r$), ($ap \times Vc$), and ($ap \times f$) on (*Fz*). As found by ANOVA, these curves show that (*ap*) has the dominant effect, followed by (*f*) and (*Vc*), while the effect of (*r*) remains almost negligible. Figure 9a demonstrates that the force (*Fz*) is minimal when (*ap*) and (*r*) are at their minimum values. Figure 9b indicates that when (*ap*) is at the lowest value and (*Vc*) at the highest one, the parameter (*Fz*) is at its minimum. According to Fig. 9c, the minimum force is obtained with low values of (*ap*) and (*f*), i.e., for a small section of the removed chip. The 3D graphs of Fig. 10a–c, allow to evaluate the simultaneous effect of ($Vc \times f$), ($Vc \times ap$), and ($ap \times r$) on (*Pc*). Figure 10a indicates an interaction between

Fig. 5 Comparison between experimental and predicted values for $(Ra, V_{ing}, F_z, \text{ and } Pc)$



the effect of (V_c) and that of (f) ; indeed, for a small value of (V_c) , the effect of (f) is negligible. Whereas for a maximum value of (V_c) , an increase in (f) leads to a considerable change in (P_c) . From Fig. 10b, the lowest value of (P_c) is reached when (ap) and (V_c) are at their low level. Figure 10c illustrates that the effect of (r) is very small before that of (ap) ; when (r) and (ap) are at their minimum value, the parameter (P_c) has the lowest value.

4 Multi-objective optimization of cutting conditions

Optimization is an important step in the machining process, which selects the most appropriate cutting conditions to obtain the required values for a single or multiple variables, which usually has a direct economic impact such as machine time or

total machining cost [51]. In this study, two multi-objective optimization methods, namely, the desirability function (DF) approach and gray relational analysis (GRA) were used. The goal is to find an optimal cutting regime that satisfies two cases, namely, $(Ra_{-min}, V_{ing_{-min}}, \text{ and } MRR_{-max})$ and $(Ra_{-min}, V_{ing_{-min}}, Fz_{-min}, Pc_{-min}, \text{ and } MRR_{-max})$.

5 Optimization by the maximization method of (DF)

The (DF) approach is a simple optimization technique that is easy to use and to program in statistical software [22, 52]. Our objective is to improve surface quality, reduce energy consumption, increase machining stability, and increase productivity simultaneously. The desirability function (DF) is defined by Eq. (7) [25, 28]:

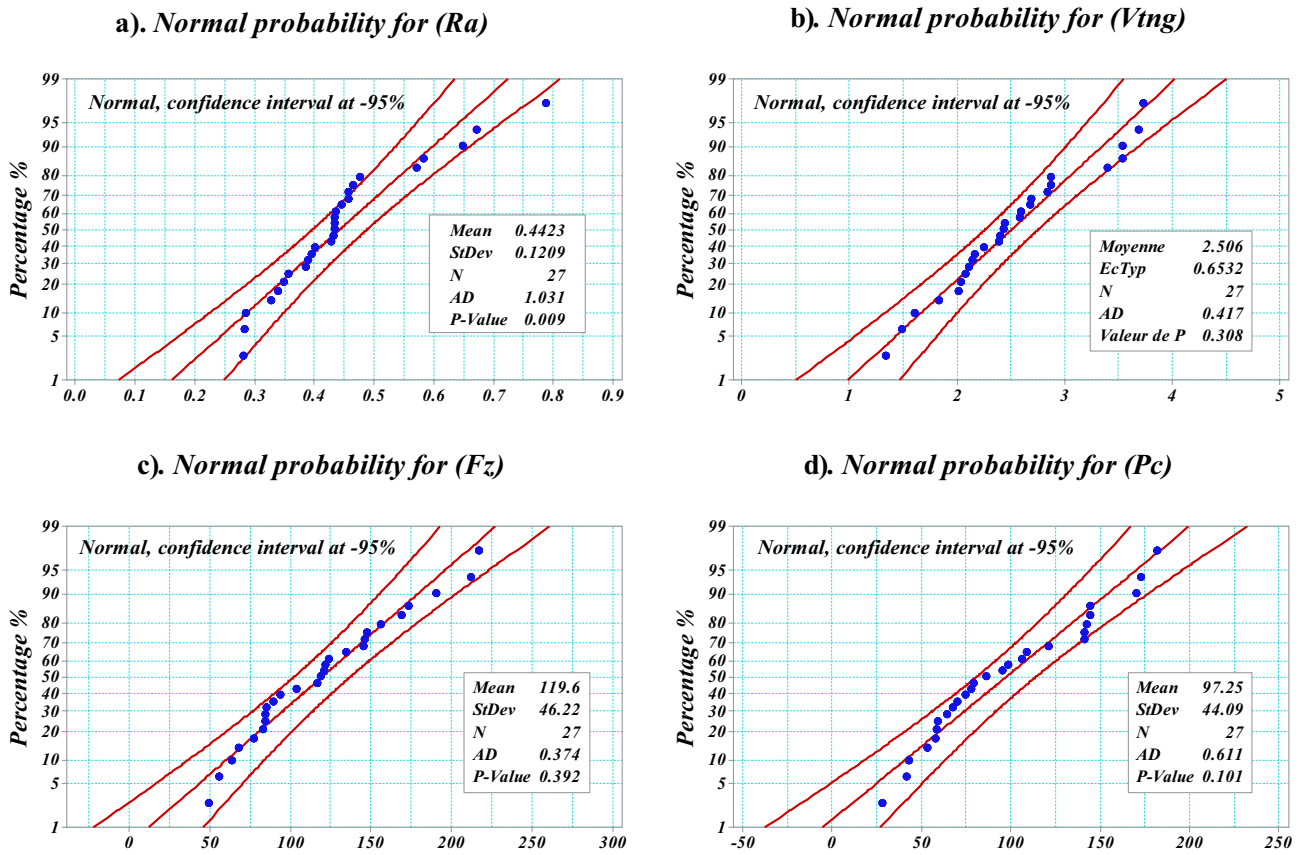


Fig. 6 Normal probability plot for (*Ra*, *Vtng*, *Fz*, and *Pc*)

$$DF = \left(\prod_{i=1}^n d_i^{w_i} \right)^{\frac{1}{\sum_{j=1}^n w_j}} \tag{7}$$

d_i: Individual desirability within [0, 1], defined by the target output, as indicated by Eqs. (8) and (9).

- n*: Number of responses in the measure;
- w_i*: Corresponding weights.

Target to maximize:

$$\begin{cases} 0 & \text{Si } Y_i \leq \min_i \\ di = \left[\frac{Y_i - \min_i}{\max_i - \min_i} \right] & \text{Si } \min_i \leq Y_i \leq \max_i \\ 1 & \text{Si } Y_i \geq \max_i \end{cases} \tag{8}$$

Target to minimize:

$$\begin{cases} 1 & \text{Si } Y_i \leq \min_i \\ di = \left[\frac{\max_i - Y_i}{\max_i - \min_i} \right] & \text{Si } \min_i \leq Y_i \leq \max_i \\ 0 & \text{Si } Y_i \geq \max_i \end{cases} \tag{9}$$

Table 8 summarizes the desired objectives and the ranges of the cutting parameters defined for the optimization, as well as

the range of variation of the considered technological parameters. Table 9 and Fig. 11 illustrate the optimization results obtained from the desirability function (DF) for the two considered cases. The optimization study of the 1st case (*Ra*-min, *Vtng*-min, and *MRR*-max) led to the regime corresponding to (*r*=0.8 mm, *Vc*=70 m/min, *f*=0.108 mm/rev, and *ap*=0.3 mm), which resulted in (*Ra*=0.297 μm, *Vtng*=2.087 m/s², and *MRR*=2.101cm³/min). While for the 2nd case (*Ra*-min, *Vtng*-min, *Fz*-min, *Pc*-min, and *MRR*-max), where all five output parameters are considered simultaneously, the optimal regime obtained is (*r*=0.8 mm, *Vc*=69.192 m/min, *f*=0.088 mm/rev, and *ap*=0.197 mm) and which resulted in the different optimized outputs (*Ra*=0.280 μm, *Vtng*=1.559 m/s², *Fz*=63.769 N, *Pc*=81.660 W, and *MRR*=0.977 cm³/min). These results indicate that taking into account (*Fz*) and (*Pc*), results in a decrease of (53.4%) in (*MRR*), caused by a reduction in the chip cross section (*ap*×*f*). On the other hand, the value of (*Ra*) remains almost unchanged, while a slight decrease in (*Vtng*) is observed.

5.1 Optimization by method (GRA)

The (GRA) method is a technique for solving difficult optimization problems by transforming the multi-objective

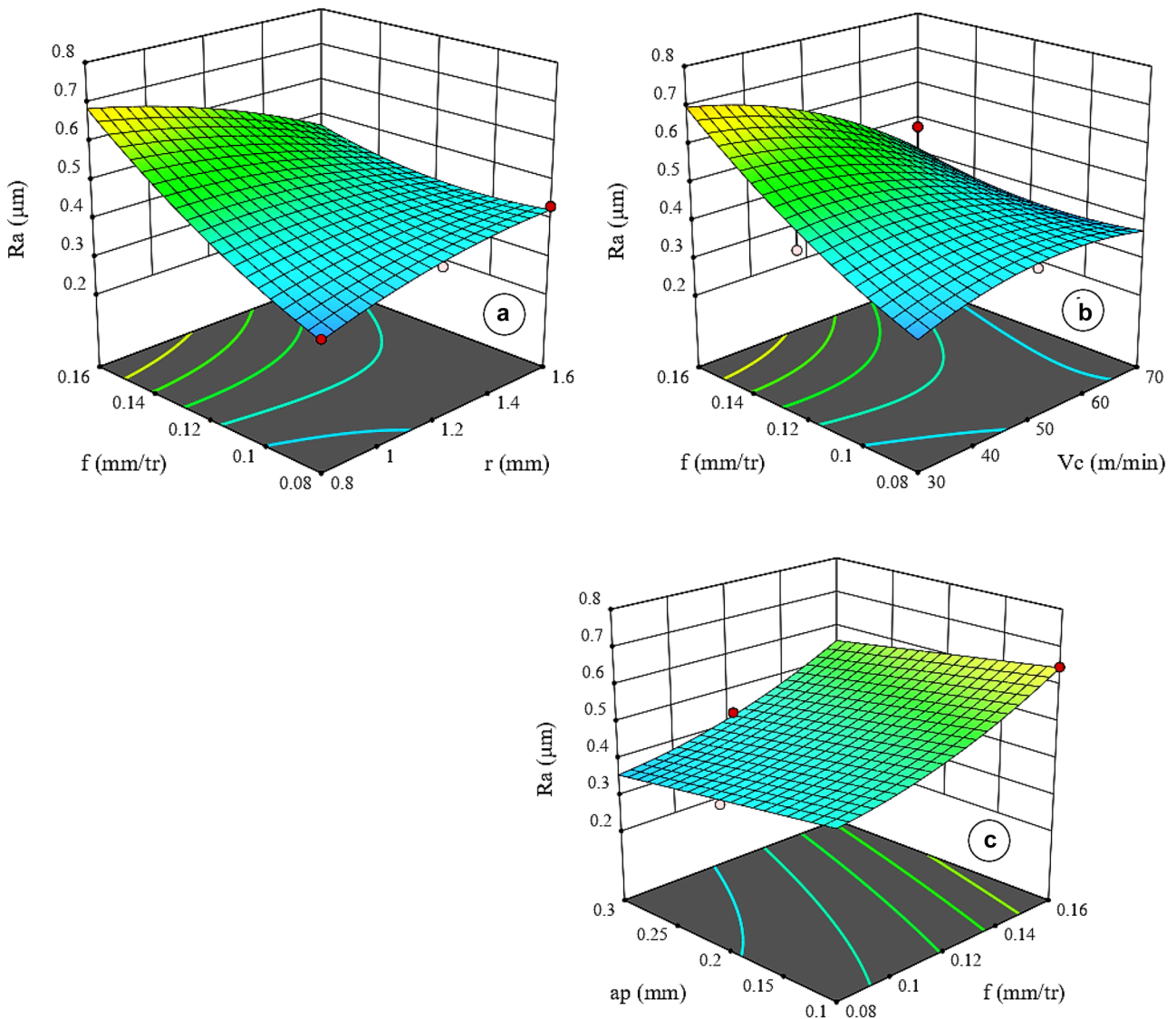


Fig. 7 3D response surface for (Ra)

problem into a single objective [30, 34]. The goal of the (GRA) method is to determine the optimal combination of turning parameters, which allows us to minimize (Ra , V_{tng} , F_z , and P_c) and maximize the (MRR), following the two cases mentioned above. The steps of the (GRA) method are presented in Fig. 12.

(a) Normalization

This step consists in normalizing the experimental results of the output parameters, according to the goal of the optimization, in order to make all the responses of the same magnitude in the interval [0–1]. For the minimization of (Ra , V_{tng} , F_z , and P_c), the normalization was performed according to

Eq. (10), and for the maximization of (MRR) by Eq. (11). The results of the normalization are reported in Table 10.

$$x_i(k) = \frac{\max(x_i^0(k)) - x_i^0(k)}{\max(x_i^0(k)) - \min(x_i^0(k))} \tag{10}$$

$$x_i(k) = \frac{x_i^0(k) - \min(x_i^0(k))}{\max(x_i^0(k)) - \min(x_i^0(k))} \tag{11}$$

where

- $x_i(k)$: Normalized value
- $\max(x_i^0(k))$: Maximum value of the (kth) response $x_i^0(k)$
- $\min(x_i^0(k))$: Minimum value of the (kth) response $x_i^0(k)$

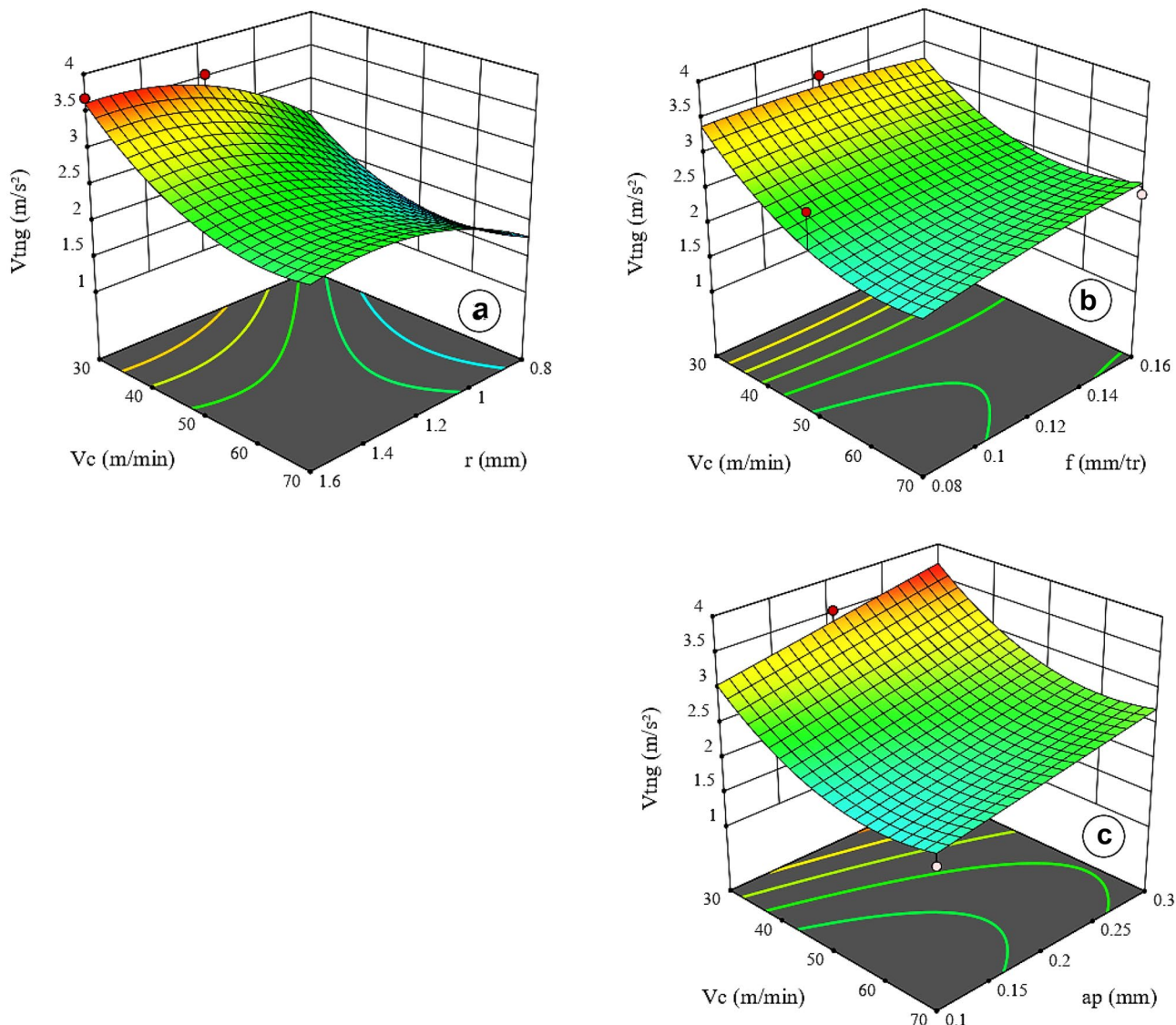


Fig. 8 3D response surface for (Vtng)

The value of $x_i(k) = 1$ of the normalized results indicates the best performance characteristic.

(b) Calculation of gray relational coefficients (GRC)

The GRC coefficient represents the correlation between the ideal and experimental results. The mathematical formula for GRC ($\xi(k)$) is given as follows:

$$GRC_i = \frac{\Delta_{min} + \Psi \Delta_{max}}{\Delta_{0i} + \Psi \Delta_{max}} \tag{12}$$

where

$\Delta_{0i}(k)$: Difference in absolute value between the ideal value $x_0^k(k)$ and $x_i^k(k)$

Δ : The smallest value of $\Delta_{0i}(k)$

Δ : The Greatest value of $\Delta_{0i}(k)$

Ψ : is the distinction coefficient ($\Psi \in [0, 1]$). In our case the value of Ψ is 0.5.

$$\Delta_{0i}(k) = \|x_0(k) - x_i(k)\| \tag{13}$$

$$\Delta_{min} = \min_{j \in i} \min_k \|x_0(k) - x_i(k)\| \tag{14}$$

$$\Delta_{max} = \max_{j \in i} \max_k \|x_0(k) - x_i(k)\| \tag{15}$$

The values of the (GRC) are presented in the Table 11.

(iii) Calculation of gray relational grade (GRG)

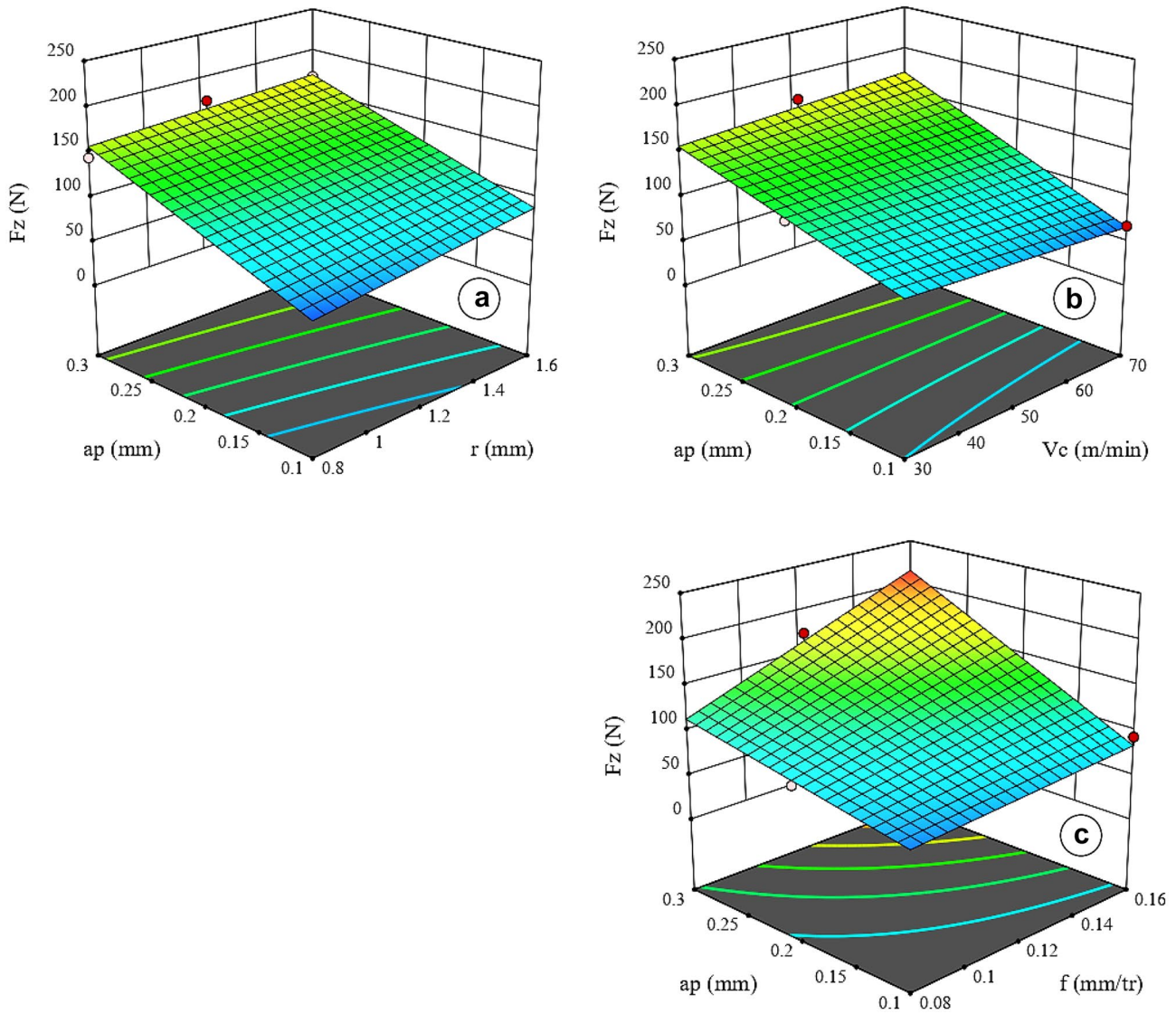


Fig. 9 3D response surface for (F_z)

The (GRG) indicates the relationship between the series, it is calculated by the Eq. (16).

$$GRG_i = \frac{1}{n} \sum_{k=1}^n GRC_i \tag{16}$$

n : is the number of performance characteristics (in our case $n=5$)

i : 1 to m , where m is the number of tests

After the GRG calculation, the optimal level combination is selected on the basis of the gray relational grade (GRG)

table. The largest GRG value that is near the ideal normalized value is the optimal combination. Consequently, the optimal level of the process parameters is the level with the largest GRG value. Table 11.

The level corresponding to the maximum of the average values of the “grey relational quality” is the optimal level of the parameters. The optimal combination of the parameters of the Inconel 718 turning process is deduced from Fig. 13.

From the main effects plot of (GRG) in Fig. 13, the optimal combination for the 1st case (Ra , V_{mg} , and MRR), the parameters are (r_1 , V_{c3} , f_2 , and ap_2). For the 2nd case (Ra , V_{mg} , F_z , P_c , and MRR), the optimal combination is (r_1 ,

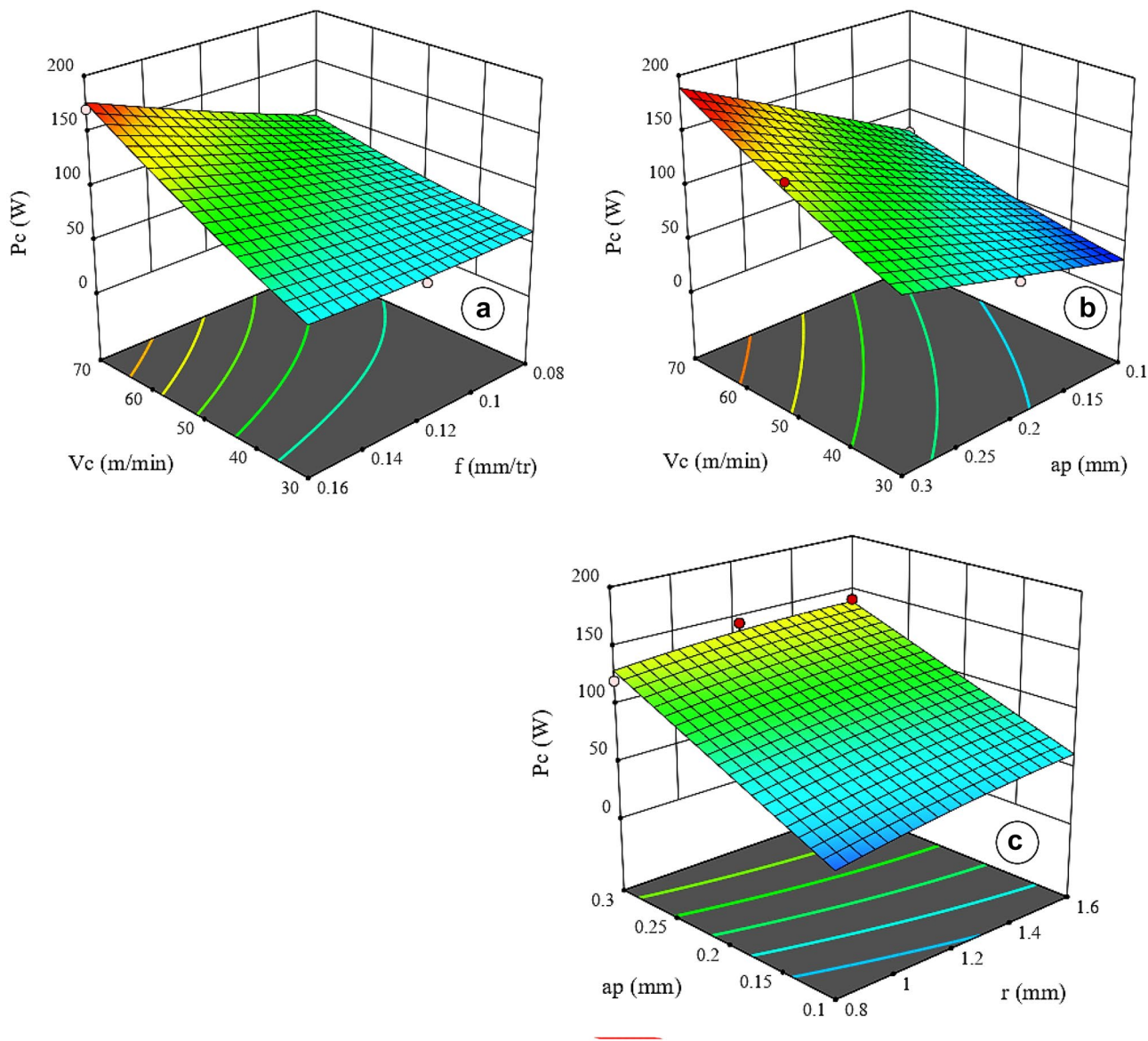


Fig. 10 3D response surface for (Pc)

$Vc3$, $f1$, and $ap1$). We note that the two optimal regimes found are not included in the L_{27} experimental design along with the corresponding output values. For this purpose,

Eq. (17) was used to calculate the predicted output values [53, 54]. The results found for the two optimization cases are reported in Table 12.

Table 8 Constraints for the two optimization cases

Response	Objective	Inferior	Target	Superior	Weighting	Importance
R (mm)	in range	0.8	*	1.6	*	*
Vc (m/min)	in range	30	*	70	*	*
f (mm/rev)	in range	0.08	*	0.16	*	*
ap (mm)	in range	0.1	*	0.3	*	*
Ra (μ m)	minimize	*	0.280	0.787	1	1
$Vtng$ (m/s^2)	minimize	*	1.334	3.728	1	1
Fz (N)	minimize	*	49.640	217.050	1	1
Pc (W)	minimize	*	27.900	181.755	1	1
MRR (cm^3/min)	maximize	0.24	2.240	*	1	1

Table 9 Results for the two optimization cases (DF)

→ no variation ↑ Increase ↓ Decrease	Optimal cutting conditions				Optimal Output Parameters					
	<i>r</i> (mm)	<i>V_c</i> (m/min)	<i>f</i> (mm/rev)	<i>ap</i> (mm)	<i>R_a</i> (μm)	<i>V_{ing}</i> (m/s ²)	<i>F_z</i> (N)	<i>P_c</i> (W)	<i>MRR</i> (cm ³ /min)	<i>DF</i>
1 st case	0.8	70	0.108	0.3	0.297	2.088	*	*	2.100	0.850
2 nd case	0.8	69.192	0.088	0.197	0.280	1.559	63.769	81.660	1.19	0.724
% change	→ 0.00 %	↓ 1.15 %	↓ 18.52 %	↓ 34.33 %	↓ 5.72 %	↓ 25.34 %	*	*	↓ 43.33 %	↓ 14.82 %

$$Pr = A_G + \sum_{j=1}^n [(A_{ij}) - A_G] \tag{17}$$

where

Pr: Predicted response value.

A_G: General average for each of the output parameters.

A_{i,j}: Average of the response at the optimal level.

n: Number of machining parameters. In this case, *n* = 4 (*r*, *V_c*, *f*, and *ap*).

Table 12 illustrates the results obtained by the method (GRA) for the two optimization cases. The 1st case (*R_a-min*, *V_{ing}-min*, and *MRR-max*) led to the regime corresponding to (*r*=0.8 mm, *V_c*=70 m/min, *f*=0.12 mm/rev, and *ap*=0.2 mm), which gives three outputs (*R_a*=0.318 μm,

V_{ing} = 1.740 m/s², and *MRR* = 1.680 cm³/min). While for the 2nd case (*R_a-min*, *V_{ing}-min*, *F_z-min*, *P_c-min*, and *MRR-max*), where all output parameters are considered simultaneously, the regime obtained is (*r*=0.8 mm, *V_c*=70 m/min, *f*=0.08 mm/rev, and *ap*=0.1 mm), which gives the following responses: (*R_a*=0.355 μm, *V_{ing}* = 1.277 m/s², *F_z* = 31.683 N, *P_c* = 74.095 W, and *MRR* = 0.56 cm³/min). The results found show that the consideration of the outputs (*F_z*) and (*P_c*) in the optimization causes a decrease of the (*MRR*) of (66.66%). On the other hand, the value of (*R_a*) undergoes a slight increase of (11.63%) and the value of (*V_{ing}*) enjoys a decrease of (26.60%). This optimization case also showed very low values for both (*F_z* and *P_c*), especially the value of (*F_z*).

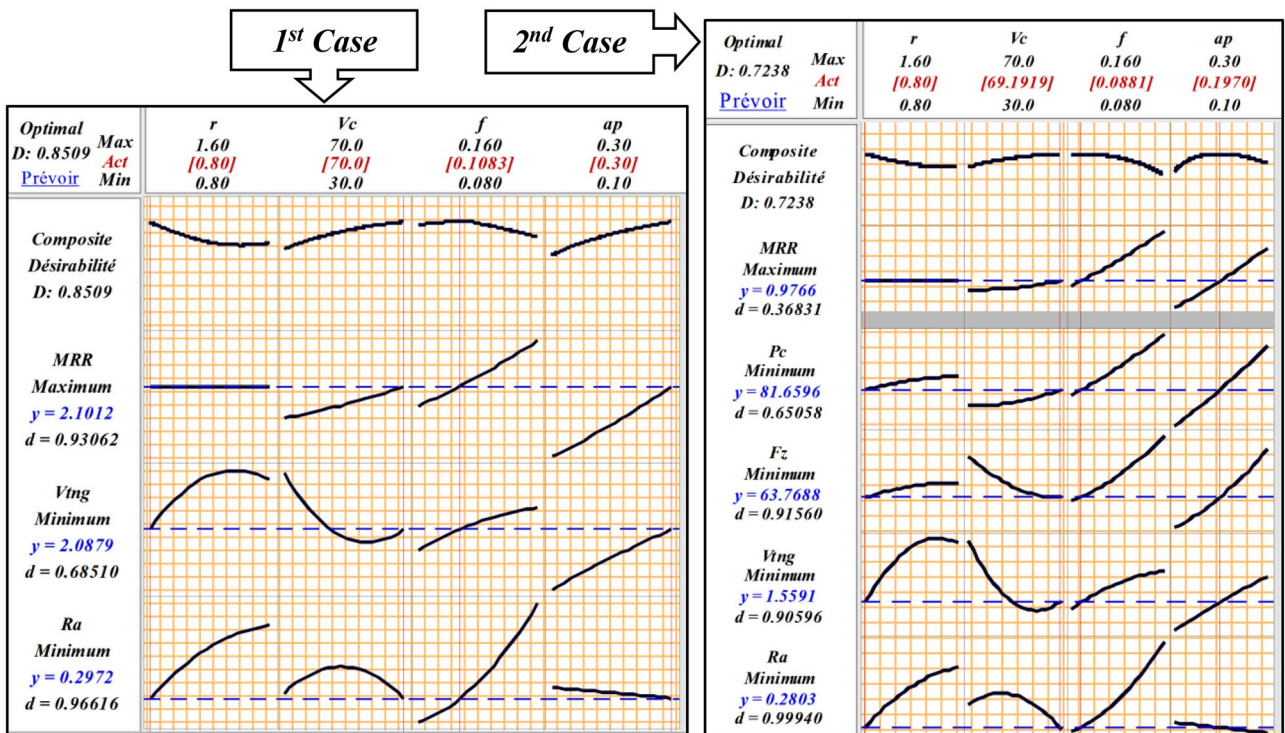


Fig. 11 Optimization diagram for the two cases

Fig. 12 Steps involved in (GRA) method

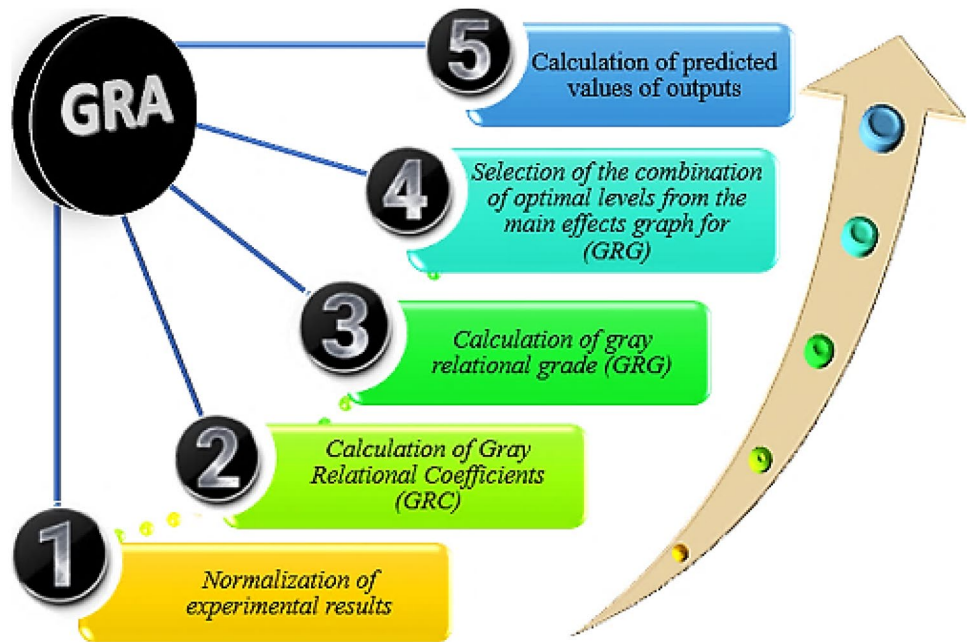


Table 10 Normalized experimental results $x_i(k)$

No. of test (i)	Ra	Vtng	Fz	Pc	MRR
<i>Ideal value</i>	1	1	1	1	1
1	0.761	0.690	0.963	1.000	0.000
2	0.426	0.619	0.589	0.796	0.240
3	0.227	0.433	0.158	0.562	0.600
4	0.905	1.000	0.837	0.765	0.280
5	0.864	0.662	0.431	0.396	0.780
6	0.000	0.888	0.916	0.836	0.280
7	1.000	0.794	0.569	0.257	0.720
8	0.886	0.937	1.000	0.805	0.300
9	0.694	0.678	0.414	0.061	1.000
10	0.651	0.358	0.787	0.904	0.000
11	0.702	0.080	0.598	0.801	0.240
12	0.404	0.000	0.000	0.476	0.600
13	0.791	0.360	0.793	0.725	0.280
14	0.698	0.441	0.263	0.244	0.780
15	0.272	0.706	0.739	0.675	0.280
16	0.708	0.543	0.575	0.265	0.720
17	0.996	0.717	0.893	0.669	0.300
18	0.613	0.538	0.424	0.074	1.000
19	0.775	0.140	0.799	0.911	0.000
20	0.783	0.019	0.493	0.744	0.240
21	0.637	0.081	0.030	0.492	0.600
22	0.696	0.656	0.677	0.620	0.280
23	0.675	0.371	0.287	0.266	0.780
24	0.651	0.555	0.764	0.698	0.280
25	0.698	0.480	0.559	0.245	0.720
26	0.848	0.562	0.792	0.541	0.300
27	0.992	0.476	0.366	0.000	1.000

Table 11 Gray relational grade coefficients ($GRC_i(k)$) and gray relational grade (GRG_i)

No. of test (i)	GRC					GRG	
	ξ_{Ra}	ξ_{Vtng}	ξ_{Fz}	ξ_{Pc}	ξ_{MRR}	1 ^{er} Cas	2 ^{ème} Cas
1	0.677	0.617	0.931	1.000	0.333	0.542	0.712
2	0.466	0.567	0.549	0.711	0.397	0.477	0.538
3	0.393	0.469	0.373	0.533	0.556	0.472	0.465
4	0.841	1.000	0.755	0.680	0.410	0.750	0.737
5	0.786	0.597	0.468	0.453	0.694	0.692	0.600
6	0.333	0.817	0.856	0.753	0.410	0.520	0.634
7	1.000	0.708	0.537	0.402	0.641	0.783	0.658
8	0.814	0.889	1.000	0.719	0.417	0.706	0.768
9	0.621	0.608	0.460	0.347	1.000	0.743	0.607
10	0.589	0.438	0.701	0.839	0.333	0.453	0.580
11	0.627	0.352	0.554	0.716	0.397	0.459	0.529
12	0.456	0.333	0.333	0.488	0.556	0.448	0.433
13	0.705	0.439	0.707	0.645	0.410	0.518	0.581
14	0.624	0.472	0.404	0.398	0.694	0.597	0.518
15	0.407	0.630	0.657	0.606	0.410	0.482	0.542
16	0.631	0.522	0.540	0.405	0.641	0.598	0.548
17	0.992	0.638	0.823	0.601	0.417	0.682	0.694
18	0.564	0.520	0.465	0.351	1.000	0.695	0.580
19	0.690	0.368	0.714	0.849	0.333	0.464	0.591
20	0.697	0.338	0.496	0.662	0.397	0.477	0.518
21	0.579	0.352	0.340	0.496	0.556	0.496	0.465
22	0.622	0.593	0.608	0.568	0.410	0.541	0.560
23	0.606	0.443	0.412	0.405	0.694	0.581	0.512
24	0.589	0.529	0.679	0.624	0.410	0.509	0.566
25	0.624	0.490	0.531	0.398	0.641	0.585	0.537
26	0.767	0.533	0.706	0.521	0.417	0.572	0.589
27	0.984	0.488	0.441	0.333	1.000	0.824	0.649

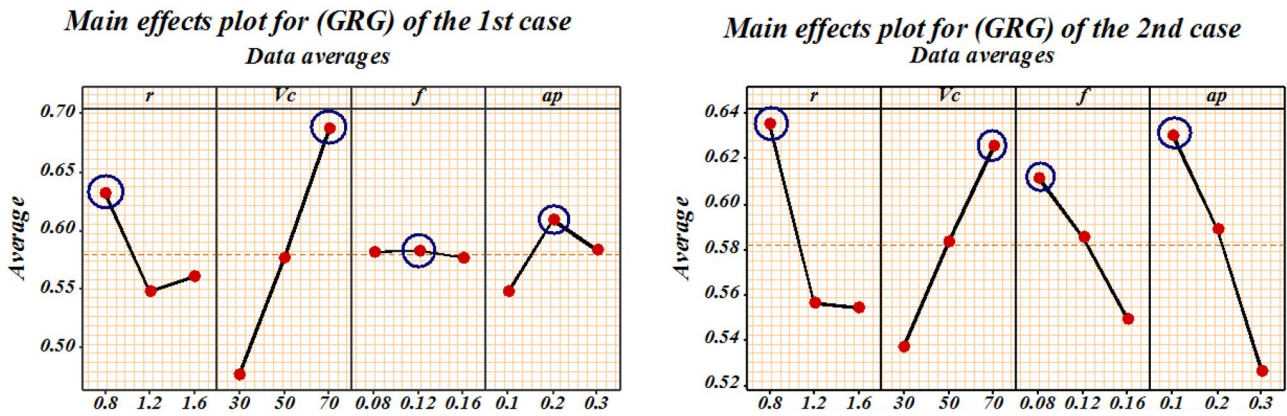


Fig. 13 Gray relational grade (GRG) main effects plot

Table 12 Results for the two optimization cases using the (GRA) method

→ no variation ↑ Increase ↓ Decrease	Optimal cutting conditions				Optimal Output Parameters				
	<i>r</i> (mm)	<i>Vc</i> (m/min)	<i>f</i> (mm/rev)	<i>ap</i> (mm)	<i>Ra</i> (μm)	<i>Vtng</i> (m/s ²)	<i>Fz</i> (N)	<i>Pc</i> (W)	<i>MRR</i> (cm ³ /min)
1 st case	0.8	70	0.12	0.2	0.318	1.740	/	/	1.680
2 nd case	0.8	70	0.08	0.1	0.355	1.277	31.683	74.095	0.56
% change	0.00 %	0.00 %	33.33 %	50.00 %	11.63 %	26.60 %	*	*	66.66 %

Table 13 Results obtained

→ no variation ↑ Increase ↓ Decrease	Parameters	1 st case			2 nd case		
		DF	GRA	% change	DF	GRA	% change
Optimal cutting conditions	<i>r</i> (mm)	0.8	0.8	→ 0.00 %	0.8	0.8	→ 0.00 %
	<i>Vc</i> (m/min)	70	70	→ 0.00 %	69.192	70	↑ 1.17 %
	<i>f</i> (mm/rev)	0.108	0.12	↑ 11.11 %	0.088	0.08	↓ 9.09 %
	<i>ap</i> (mm)	0.3	0.2	↓ 33.33 %	0.197	0.1	↓ 49.24 %
Optimal Output Parameters	<i>Ra</i> (μm)	0.297	0.318	↑ 7.07 %	0.280	0.355	↑ 26.79 %
	<i>Vtng</i> (m/s ²)	2.087	1.740	↓ 16.63 %	1.559	1.277	↓ 18.09 %
	<i>Fz</i> (N)	*	*	*	63.769	31.683	↓ 50.32 %
	<i>Pc</i> (W)	*	*	*	81.660	74.095	↓ 9.26 %
	<i>MRR</i> (cm ³ /min)	2.268	1.680	↓ 25.93 %	1.199	0.56	↓ 53.29 %

5.2 Comparisons between the two optimization methods (DF) and (GRA)

Table 13 exposes the results of the optimal cutting regimes as well as the values of the outputs for the two optimization cases obtained by the two methods (DF) and (GRA). The comparison of the optimal regimes obtained for the 1st

case shows that the factors (*r* and *Vc*) are the same, but (*f*) increased by (0.108 to 0.12) mm/rev, and (*ap*) decreased by (0.3 to 0.2) mm, for (DF) and (GRA) respectively. This led to low roughness (*Ra*) and maximum (*MRR*) for (DF) method; on the other side, the tool vibration (*Vtng*) is lower for (GRA) method. The comparison for the 2nd optimization case indicates that the (DF) method favors the

minimization of (Ra) by (21.12%) for a better surface quality as it increased by (26.79%) compared to (GRA). Similarly, (DF) improves (MRR) by (114.10%), for maximum production, as it decreased by (53.29%) compared to (GRA). In contrast, the (GRA) method favors the minimization of the parameters ($Vtng$, Fz , and Pc) compared to (DF) by (18.09%, 50.32%, and 9.26%) respectively.

6 Conclusion

The experimental, modeling, and optimization study in finishing turning of Inconel 718 by a coated metal carbide tool (GC1105) led to the following conclusions:

1. The ANOVA of (Ra), indicates that the main factors are significant. The feed rate (f) has the greatest influence with a cont% of (23.39%), followed by (Vc) and the radius (r) with cont% of (16.09% and 3.7%) respectively, lastly, the factor (ap) with a cont% of (0.02%). The terms ($Vc \times Vc$), ($r \times Vc$), ($r \times f$), ($Vc \times f$), and ($Vc \times ap$) are also significant.
2. The ANOVA of ($Vtng$) reveals that the main terms (Vc , r , and ap) are significant. The radius (r) has the greatest influence with a cont% of (32.41%), (Vc) with a cont% of (31.36%), the depth (ap) with a cont% of (8.77%), and lastly, the factor (f) with a cont% of (1.28%). The square terms ($r \times r$) and ($Vc \times Vc$) are also significant with cont% of (6.23% and 9.41%) respectively.
3. The ANOVA of (Fz) proves that the main factors are significant, and that the factor (ap) has the highest cont% with (64.11%), followed by the factor (f) with a cont% of (21.18%), then comes (Vc) and (r) with cont% of (3.86% and 3.46%) respectively. Note also that all the square terms are significant, as well as the two interactions ($Vc \times f$) and ($Vc \times ap$).
4. The ANOVA of (Pc) indicates that all four main factors are significant and that (ap) is the most important factor affecting (Pc) with (38.29%) cont%. On the other side, the factors (Vc , f , and r) have cont% of (36.99%, 8.59%, and 2.41%) respectively. The interaction ($Vc \times f$) is significant with (9.22%) cont%.
5. The mathematical models of the output parameters (Ra , $Vtng$, Fz , and Pc) proposed in this study were found to be accurate, all (R^2) are high, ($R^2_{Ra} = 92.02\%$), ($R^2_{Vtng} = 92.96\%$), ($R^2_{Fz} = 98.32\%$), and ($R^2_{Pc} = 98.45\%$). They can be used for the best predictions of the responses as well as for optimization.
6. Optimization using the (DF) approach was applied on the basis of the mathematical models found, following two desired objectives. The optimal cutting regimes are as follows:

- (a) 1st case: For minimization of (Ra and $Vtng$) and maximization of (MRR):
($r = 0.8$ mm, $Vc = 70$ m/min, $f = 0.108$ mm/rev, $ap = 0.3$ mm), corresponding to the optimized output values, ($Ra = 0.297$ μm , $Vtng = 2.087$ m/s^2 , and $MRR = 2.268$ cm^3/min).
- (b) 2nd case: For minimization of (Ra , $Vtng$, Fz , and Pc) and maximization of (MRR):
($r = 0.8$ mm, $Vc = 69.192$ m/min, $f = 0.088$ mm/rev, $ap = 0.197$ mm), which correspond to the optimized of output values, $Ra = 0.280$ μm , $Vtng = 1.559$ m/s^2 , $Fz = 63.769$ N, $Pc = 81.660$ W, and $MRR = 1.199$ cm^3/min .

7. The optimization using the (GRA) approach was applied following the same desired objectives as the (DF) optimization method. The optimal cutting regimes are as follows:

- (a) 1st case: For minimization of (Ra and $Vtng$) and maximization of (MRR):
($r = 0.8$ mm, $Vc = 70$ m/min, $f = 0.12$ mm/rev, $ap = 0.2$ mm), which correspond to the optimized of outputs values, $Ra = 0.318$ μm , $Vtng = 1.740$ m/s^2 , and $MRR = 1.680$ cm^3/min .
- (b) 2nd case: For minimization of (Ra , $Vtng$, Fz , and Pc) and maximization of (MRR):
($r = 0.8$ mm, $Vc = 70$ m/min, $f = 0.08$ mm/rev, $ap = 0.1$ mm), which correspond to the optimized of output values, $Ra = 0.355$ μm , $Vtng = 1.277$ m/s^2 , $Fz = 31.683$ N, $Pc = 74.095$ W, and $MRR = 0.56$ cm^3/min .

8. The comparison of the optimal regimes obtained by the two methods (DF and GRA) for the 2nd optimization case indicates that the method (DF) favors the minimization of (Ra) by (21.12%), for a better surface quality, as well as the maximization of (MRR) with an increase of (114.10%). On the other hand, the (GRA) method favors the minimization of the parameters ($Vtng$, Fz , and Pc) by (18.09%, 50.32%, and 9.26%) respectively.

The present work is by no means exhaustive. It can be extended to the study of the performance gap of tool materials such as ceramics and CBN when machining Inconel 718. Further investigations can be carried out to evaluate the influence of the cutting conditions on the machining technology parameters, and particularly the cutting temperature and the wear of the cutting tools under (MQL) environment. Finally, the application of other modeling and optimization methods (such as SVM, ANN, FL, GA, PSO, and PCA) would lead to better control of the performance parameters.

Funding The present research was undertaken by the “Metal Cutting Research Group” of the Structures and Mechanics Laboratory (LMS) of the 8 May 1945-Guelma University, Algeria, and received funding from the General Directorate of Scientific Research and Technological Development (DGRSDT) under the PRFU research project A11N01UN240120190001.

Availability of data and material Not applicable.

Code availability Not applicable.

Declarations

Ethics approval I certify that the paper follows the guidelines stated in the journal’s “Ethical Responsibilities of Authors.”

Consent to participate Not applicable.

Consent for publication Ilyas Kouahla authorizes the publication of the manuscript.

Competing interests Not applicable.

Additional declarations for articles in life science journals that report the results of studies involving humans and/or animals Not applicable.

References

- Thakur A, Gangopadhyay S (2016) State-of-the-art in surface integrity in machining of nickel-based super alloys. *Int J Mach Tools Manuf* 100:25–54
- De Bartolomeis A, Newman ST, Jawahir IS, Biermann D, Shokrani A (2021) Future research directions in the machining of Inconel 718. *J Mater Process Technol* 297:117260
- Roy S, Kumar R, Panda A, Das RK (2018) A brief review on machining of Inconel 718. *Materials Today: Proceedings* 5(9):18664–18673
- Dudzinski D, Devillez A, Moufki A, Larrouquere D, Zerrouki V, Vigneau J (2004) A review of developments towards dry and high speed machining of Inconel 718 alloy. *Int J Mach Tools Manuf* 44(4):439–456
- Devillez A, Le Coz G, Dominiak S, Dudzinski D (2011) Dry machining of Inconel 718, workpiece surface integrity. *J Mater Process Technol* 211(10):1590–1598
- Cantero JL, Díaz-Álvarez J, Miguélez MH, Marín NC (2013) Analysis of tool wear patterns in finishing turning of Inconel 718. *Wear* 297(1–2):885–894
- Park KH, Yang GD, Lee DY (2015) Tool wear analysis on coated and uncoated carbide tools in Inconel machining. *Int J Precis Eng Manuf* 16(7):1639–1645
- Rahman M, Seah WKH, Teo TT (1997) The machinability of Inconel 718. *J Mater Process Technol* 63(1–3):199–204
- Mahesh K, Philip JT, Joshi SN, Kuriachen B (2021) Machinability of Inconel 718: a critical review on the impact of cutting temperatures. *Mater Manuf Process* 36(7):753–791
- Behera GC, Thrinadh J, Datta S (2021) Influence of cutting insert (uncoated and coated carbide) on cutting force, tool-tip temperature, and chip morphology during dry machining of Inconel 825. *Materials Today: Proceedings* 38:2664–2670
- Deshpande Y, Andhare A, Sahu NK (2017) Estimation of surface roughness using cutting parameters, force, sound, and vibration in turning of Inconel 718. *J Braz Soc Mech Sci Eng* 39(12):5087–5096
- Tebassi H, Yaltese M, Belhadi S, Girardin F, Mabrouki T (2017) Quality-productivity decision making when turning of Inconel 718 aerospace alloy: a response surface methodology approach. *Int J Ind Eng Comput* 8(3):347–362
- Thirumalai R, Seenivasan M, Panneerselvam K (2021) Experimental investigation and multi response optimization of turning process parameters for Inconel 718 using TOPSIS approach. *Mater Today Proc* 45:467–472
- Deshpande YV, Andhare AB, Padole PM (2019) Application of ANN to estimate surface roughness using cutting parameters, force, sound and vibration in turning of Inconel 718. *SN Appl Sci* 1(1):1–9
- Tan L, Yao C, Li X, Fan Y, Cui M (2022) Effects of machining parameters on surface integrity when turning Inconel 718. *J Mater Eng Perform* 1–11
- Alsorujji G, Muthuramalingam T, Moustafa EB, Elsheikh A (2022) Investigation and TGRA based optimization of laser beam drilling process during machining of Nickel Inconel 718 alloy. *J Market Res* 18:720–730
- Xu D, Liu Y, Ding L, Zhou J, M’Saoubi R, Liu H (2022) Experimental and numerical investigation of Inconel 718 machining with worn tools. *J Manuf Process* 77:163–173
- Sivalingam V, Poogavanam G, Natarajan Y, Sun J (2021) Optimization of atomized spray cutting fluid eco-friendly turning of Inconel 718 alloy using ARAS and CODAS methods
- Zahoor S, Abdul-Kader W, Shehzad A, Habib MS (2022) Milling of Inconel 718: an experimental and integrated modeling approach for surface roughness. *Int J Adv Manuf Technol* 1–16
- Zolpakar NA, Yasak MF, Pathak S (2021) A review: use of evolutionary algorithm for optimisation of machining parameters. *Int J Adv Manuf Technol* 115(1):31–47
- Chakraborty S, Chakraborty S (2022) A scoping review on the applications of MCDM techniques for parametric optimization of machining processes. *Arch Comput Methods Eng* 1–22
- Bhaskar P, Sahoo SK (2020) Optimization of machining process by desirability function analysis (DFA): a review. *CVR J Sci Technol* 18(1):138–143
- Frifita W, Salem SB, Haddad A, Yaltese MA (2020) Optimization of machining parameters in turning of Inconel 718 nickel-base super alloy. *Mech Ind* 21(2):203
- Tebassi H, Yaltese M, Khettabi R, Belhadi S, Meddour I, Girardin F (2016) Multi-objective optimization of surface roughness, cutting forces, productivity and power consumption when turning of Inconel 718. *Int J Ind Eng Comput* 7(1):111–134
- Parida AK, Maity KP (2016) Optimization in hot turning of nickel based alloy using desirability function analysis. *Int J Eng Res Africa* 24:64–70. Trans Tech Publications Ltd
- Kuppan P, Rajadurai A, Narayanan S (2008) Influence of EDM process parameters in deep hole drilling of Inconel 718. *Int J Adv Manuf Technol* 38(1):74–84
- Kar T, Mandal NK, Singh NK (2020) Multi-response optimization and surface texture characterization for CNC milling of Inconel 718 alloy. *Arab J Sci Eng* 45(2):1265–1277
- Manohar M, Joseph J, Selvaraj T, Sivakumar D (2013) Application of desirability-function and RSM to optimise the multi-objectives while turning Inconel 718 using coated carbide tools. *Int J Manuf Technol Manag* 27(4–6):218–237
- Świercz R, Oniszczuk-Świercz D, Chmielewski T (2019) Multi-response optimization of electrical discharge machining using the desirability function. *Micromachines* 10(1):72
- Maiyar LM, Ramanujam R, Venkatesan K, Jerald J (2013) Optimization of machining parameters for end milling of Inconel 718 super alloy using Taguchi based grey relational analysis. *Procedia Eng* 64:1276–1282

31. Karsh PK, Singh H (2018) Multi-characteristic optimization in wire electrical discharge machining of Inconel-625 by using Taguchi-grey relational analysis (GRA) approach: optimization of an existing component/product for better quality at a lower cost. *Des Optim Mech Eng Prod* 281–303. IGI Global
32. Sanghvi N, Vora D, Patel J, Malik A (2021) Optimization of end milling of Inconel 825 with coated tool: a mathematical comparison between GRA, TOPSIS and Fuzzy Logic methods. *Mater Today Proc* 38:2301–2309
33. Vikram KA, Lakshmi VVK, Praveen AV (2018) Evaluation of process parameters using GRA while machining low machinability material in dry and wet conditions. *Mater Today Proc* 5(11):25477–25485
34. Sahu AK, Mohanty PP, Sahoo SK (2017) Electro discharge machining of Ti-alloy (Ti6Al4V) and 316L stainless steel and optimization of process parameters by grey relational analysis (GRA) method. *Adv 3D Print Add Manuf Technol* 65–78. Springer, Singapore
35. Kant R, Dharmi SS (2021) Multi-response optimization of parameters using GRA for abrasive water jet machining of EN31 steel. *Mater Today Proc* 47:6141–6146
36. Moharana BR, Patro SS (2019) Multi objective optimization of machining parameters of EN-8 carbon steel in EDM process using GRA method. *Int J Modern Manuf Technol* 11(2):50–56
37. Pradhan MK (2013) Estimating the effect of process parameters on MRR, TWR and radial overcut of EDMed AISI D2 tool steel by RSM and GRA coupled with PCA. *Int J Adv Manuf Technol* 68(1):591–605
38. Hanif M, Ahmad W, Hussain S, Jahanzaib M, Shah AH (2019) Investigating the effects of electric discharge machining parameters on material removal rate and surface roughness on AISI D2 steel using RSM-GRA integrated approach. *Int J Adv Manuf Technol* 101(5):1255–1265
39. Chaudhari R, Vora J, Parikh DM, Wankhede V, Khanna S (2020) Multi-response optimization of WEDM parameters using an integrated approach of RSM–GRA analysis for pure titanium. *J Inst Eng (India) Ser D* 101(1):117–126
40. Yaser EM, Shunmugesh K (2019) Multi-objective optimization of milling process parameters in glass fibre reinforced polymer via grey relational analysis and desirability function. *Mater Today Proc* 11:1015–1023
41. Coromant S, Catalogue M (2017) The official website of Sandvik Coromant
42. Chaurasia A, Wankhede V, Chaudhari R (2019) Experimental investigation of high-speed turning of INCONEL 718 using PVD-coated carbide tool under wet condition. *Innov Infrastruct* 367–374. Springer, Singapore
43. Pawade RS, Joshi SS (2011) Multi-objective optimization of surface roughness and cutting forces in high-speed turning of Inconel 718 using Taguchi grey relational analysis (TGRA). *Int J Adv Manuf Technol* 56(1):47–62
44. Waghmode SP, Dabade UA (2019) Optimization of process parameters during turning of Inconel 625. *Mater Today Proc* 19:823–826
45. Meddour I, Yallese MA, Aouici H (2014) Investigation and modeling of surface roughness of hard turned AISI 52100 steel: Tool vibration consideration. *Conf Multiphys Model Simul Syst Des* 419–431. Springer, Cham
46. Meddour I, Yallese MA, Bensouilah H, Khellaf A, Elbah M (2018) Prediction of surface roughness and cutting forces using RSM, ANN, and NSGA-II in finish turning of AISI 4140 hardened steel with mixed ceramic tool. *Int J Adv Manuf Technol* 97(5):1931–1949
47. Labidi A, Tebassi H, Belhadi S, Khettabi R, Yallese MA (2018) Cutting conditions modeling and optimization in hard turning using RSM, ANN and desirability function. *J Fail Anal Prev* 18(4):1017–1033
48. Zerti A, Yallese MA, Meddour I, Belhadi S, Haddad A, Mabrouki T (2019) Modeling and multi-objective optimization for minimizing surface roughness, cutting force, and power, and maximizing productivity for tempered stainless steel AISI 420 in turning operations. *Int J Adv Manuf Technol* 102(1):135–157
49. Khanna N, Agrawal C, Dogra M, Pruncu CI (2020) Evaluation of tool wear, energy consumption, and surface roughness during turning of Inconel 718 using sustainable machining technique. *J Market Res* 9(3):5794–5804
50. Chihaoui S, Yallese MA, Belhadi S, Belbah A, Safi K, Haddad A (2021) Coated CBN cutting tool performance in green turning of gray cast iron EN-GJL-250: modeling and optimization. *Int J Adv Manuf Technol* 113(11):3643–3665
51. Sharma R, Jha BK, Pahuja V (2022) Optimization techniques for response predication in metal cutting operation: a review. *Proc Int Conf Ind Manuf Syst (CIMS-2020)* 77–92. Springer, Cham
52. Roy R, Ghosh SK, Kaisar TI, Ahmed T, Hossain S, Aslam M, Rahman MM (2022) Multi-response optimization of surface grinding process parameters of AISI 4140 alloy steel using response surface methodology and desirability function under dry and wet conditions. *Coatings* 12(1):104
53. Moganapriya C, Rajasekar R, Sathish Kumar P, Mohanraj T, Gobinath VK, Saravanakumar J (2021) Achieving machining effectiveness for AISI 1015 structural steel through coated inserts and grey-fuzzy coupled Taguchi optimization approach. *Struct Multidiscip Optim* 63(3):1169–1186
54. Alagarsamy SV, Raveendran P, Ravichandran M (2021) Investigation of material removal rate and tool wear rate in spark erosion machining of Al-Fe-Si alloy composite using Taguchi coupled TOPSIS approach. *Silicon* 13(8):2529–2543

Publisher's note Springer Nature remains neutral with regard to jurisdictional claims in published maps and institutional affiliations.

Springer Nature or its licensor holds exclusive rights to this article under a publishing agreement with the author(s) or other rightsholder(s); author self-archiving of the accepted manuscript version of this article is solely governed by the terms of such publishing agreement and applicable law.